PCCP

Accepted Manuscript

ROYAL SOCIETY OF CHEMISTRY

www.rsc.org/pccp

Solvent effects and potential of mean force: A multilayered-representation quantum mechanical/molecular mechanics study of the $CH_3Br + CN^-$ reaction in aqueous solution

Yulong Xu[ab], Jingxue Zhang[a], Dunyou Wang[*a]

[a]College of Physics and Electronics, Shandong Normal University, Jinan 250014, China

[b]School of Science, Qilu University of Technology, Jinan, 250353, China

[*] Author to whom correspondence should be addressed. Email: dywang@sdnu.edu.cn

ABSTRACT

The bimolecular nucleophilic substitution (S_N2) reaction of CH_3Br and CN^- in aqueous solution was investigated using a multilayered-representation quantum mechanical and molecular mechanics methodology. Reactant complex, transition state, and product complex are identified and characterized in aqueous solution. The potentials of mean force are computed under both the DFT and CCSD(T) levels of theory for the reaction region. The CCSD(T)/MM level of theory presents a free energy activation barrier height at 19.1 kcal/mol which agrees very well with the experiment value at 20.7 kcal/mol, while the DFT/MM level of theory underestimated the barrier height at 16.5 kcal/mol. The results show that the aqueous environment has a significant contribution to the potential of mean force. The solvation effect and the polarization effect combined increases the activation barrier height by ~14.5 kcal/mol and the solvation effect plays a major role by providing about 70% of the contribution.

I. INTRODUCTION

Bimolecular nucleophilic substitution (S_N2) is a fundamental reaction in organic chemistry. Certain characters of the S_N2 reaction in gas phase have been well established. For example, for the $CH_3X + Y^- \rightarrow CH_3Y + X^-$ (X and Y are halogen atoms) reactions, both theoretical and experimental studies show that the preferred gas-phase reaction pathway of such reactions involves a backside attack of the substrate, followed by the "Walden inversion" of the CH_3 group[1-5]. The potential energy profile can be characterized by two wells in the reactants' and products' valleys arising from the strong ion-molecule attractive force, and separated by a central barrier[6-8]; unlike in gas phase, the minima are usually disappeared[9-13] on the potential energy surface(PES) in solution phase, and the activation barriers of these reactions are strongly affected by solvent[14-19]. Recent work has shown a non-traditional reaction path which involves hydrogen-bonding of attacking anion[20,21]. In addition to the backside attack mechanism, there are also stripping and roundabout mechanisms[22-25]. Nonetheless, the interests of these S_N2 reactions have been mostly focused on the gas phase in the past several decades, theoretical studies, especially to quantitatively determine the solvent effects and to accurately map the potential of mean force in the solution phase, are limited. In contrast to reactions in gas phase, the solvent alters the reaction energetics in solution phase, thus a solvent medium can affect the reaction rates substantially by change the activation barrier. For instance, for the $OH^- + CH_3Br \rightarrow Br^- + CH_3OH$[26] reaction, the rate measured by Bohme and Mackay using the flowingafterglow technique is $(1.0\pm0.2) \times10^{-9}$ $cm^3molecule^{-1}s^{-1}$ in gas phase but is significantly reduced to 2.3×10^{-25} $cm^3molecule^{-1}s^{-1}$ in solution phase; furthermore, solvent molecules may take part in the reaction thus change the reaction mechanism. So understanding S_N2 reactions in solution is practical and conceptual importance to understand the reaction mechanism of these reactions and the role of the solution plays on the reaction energetics in solution phase.

For the reaction $CH_3Br + CN^-$ in gas phase, there are two experimental data available on the activation barriers which are quite different from each other: one is 8.9 kcal/mol[27], the other is 2.4±0.2

kcal/mol[28]. A theoretical calculation by Safi[29] et al. using the Hartree-Fock/6-31+G* level of theory gives the reaction barrier height at 8.19 kcal mol^{-1}, which agrees well with the former experimental value. For this reaction in solution, experimentally, a free activation barrier of 20.7±0.23 $kcalmol^{-1}$ has been determined by Moelwyn-Hugh's group[30]; theoretically, so far as we know, there have been no theoretical studies of the $CH_3Br + CN^-$ reaction in solution. Thus, in this study, we want to carry out the first theoretical calculation on the title reaction to investigate the reactant complex, transition state and product complex of this reaction in aqueous solution, to construct the reaction pathway for this reaction, to determine the potential of mean force (PMF) for the reaction $CH_3Br + CN^-$ in aqueous solution, to investigate the aqueous solution contributions to the PMF and to find what role the solution plays for the title reaction in aqueous solution.

Putting a reaction system into solution introduces hundreds or thousands of extra degrees of freedom into the system. Using pure quantum mechanical methods to treat the whole reaction system is an impossible task; moreover, the calculation of free energy in solution is also a formidable problem because it needs a huge amount of sampling of solvent configuration. So in practice, the quantum-mechanical(QM) and molecular mechanics(MM) methods are usually combined to deal with the systems in solution. The hybrid QM/MM methodology[31-33] can be partitioned into an electronically important region to which the quantum mechanical treatment is applied and the remainder (the solvent), acting in a perturbative fashion, to which the molecular mechanics is applied.

In this study, we want not only to study the properties of the stationary structures, but also to study the reaction energetics along the reaction pathway, and to map an accurate potential mean force. Therefore, we employ the explicit water model to deal with the water environment. Furthermore, utilizing a multilayered representation to treat the QM region with DFT[34], CCSD(T)[35,36] and electrostatic potential (ESP)[37] theories at different stages of the calculation, we can start the computation at the less expensive levels of theory(DFT and ESP) and at the end shift the computation to the expensive but accurate level of theory (CCSD(T)) to achieve a high accurate potential of mean force

(PMF) at the CCSD(T) level theory. In this paper, the S_N2 reaction $CH_3Br + CN^- \rightarrow CH_3CN + Br^-$ in water is investigated using the multilayered, QM/MM approach: to determine the reactant, transition state and product complexes, to investigate the detailed reaction mechanism of this reaction in solution, to quantitatively obtain the aqueous environment effect to the reaction energetics, to calculate the accurate potential of mean force on the CCSD(T)/MM level of theory and compare with experiment result.

II. METHODOLOGY AND SYSTEM SETUP

We use the QM/MM capabilities[38,39] of NWChem computational chemistry package[40] to simulate the reaction $CH_3Br + CN^- \rightarrow CH_3CN + Br^-$ in aqueous solution. More importantly, the multilayered-representation approach is applied to obtain the PMF on the accurate CCSD(T) level of theory. In this treatment, the solute $CH_3Br + CN^-$ is treated as the QM region and the water environment as the MM region. The energy of the whole system can be expressed as,

$$E = E_{qm}^{int}(r;\psi) + E_{qm}^{ext}(r,R;\rho) + E_{mm}(r,R) \quad (1)$$

Where *r, R* (should be bold) are the coordinates of the QM and MM regions respectively, and ψ denotes the ground state many-electron wave function of the solute (QM) region. Here the energy E_{qm}^{int} represents the energy of the QM region studied using quantum mechanics method, which has the expression of the energy in the gas phase. The second term of the QM energy in Eq. (1) describes the van der Waals, Coulomb solute and solvent nuclear interaction and the electrostatic interactions between the QM and MM regions. The electrostatic interaction energy between the solute electron density ρ and classical charges of water can be approximated as[37],

$$\sum_I \int \frac{Z_I \rho(r')}{|R_I - r'|} dr' = \sum_{i,I} \frac{Z_I Q_i}{|R_I - r_i|} = E_{esp}(r,R,Q) \quad (2)$$

Here the solute electron density is replaced by the effective classical charge representation (ESP) which is the bottom-level theory for the QM region of the multi-layered representations. The third term $E_{mm}(r,R)$ describes the energy of the MM region investigated using molecular mechanics method,

which is calculated under the ESP/MM representation.

Due to huge computation cost of the CCSD(T) level calculation, direct QM/MM calculation under the CCSD(T)/MM is impractical, thus multilayered QM/MM representations consisting of CCSD(T)/MM, DFT/MM, and ESP/MM are utilized in this work. We treat the QM region using CCSD(T), DFT and ESP levels of theory, respectively. The desired free energy difference ΔW_{AB} between two consecutive points A and B along a given reaction pathway at the CC/MM level of theory can then be described as[37]

$$\Delta W_{AB} = (\Delta W_{AA}^{CC\to DFT} - \Delta W_{BB}^{CC\to DFT}) + (\Delta W_{AA}^{DFT\to ESP} - \Delta W_{BB}^{DFT\to ESP}) + \Delta W_{AB}^{MM} \quad (3)$$

By doing so, we shift the description of the QM region from the ESP representation to the DFT representation, then from DFT to the CCSD(T) representation at the fixed solute configuration (A or B). Note the sum of the first two terms in the brackets is the internal energy of the solute under the CCSD(T) representation; the sum of the last two terms is the PMF under the DFT/MM level of theory. Under the classical ESP/MM description, ΔW_{AB}^{ESP} is calculated through explicit statistical sampling for changing solute configuration A to B.

In this study, the solute QM region (CH_3Br and CN^-) was embedded into a 36.2 Å cubic box with 1603 SPC/E[41] solvent water molecules representing the MM region. The solute QM region was treated using the B3LYP[42, 43] exchange correlation function, and the aug-cc-pvDZ basis is used for both the DFT and CCSD(T) levels of theory during different stages of the computation. The van der Waals parameters for the quantum region were taken from Standard Amber force field[44]. The cutoff radius for classical interactions based on SPC/E model is 15 Å.

First, the QM and MM regions were both optimized using a multi-region optimization protocol after embedding the solute into water solution. Then, the QM region was fixed and the solvent MM region was equilibrated for relaxation using the molecular dynamics simulation for 40 Picoseconds at 298 K. After the equilibration, the full system was once more optimized in water, thus the reactant complex structure was obtained. Then, according to the SN2 reaction mechanism by the breaking of the C-Br bond in the reactant complex and forming of the C-C bond in the product complex, the product complex

was searched and obtained. The searched product complex was also equilibrated and optimized as the reactant complex was.

Based on the above obtained initial reactant and product complexes, the nudged elastic band (NEB)[45,46] approach was adopted to search the reaction saddle point. An initial reaction pathway connecting the initial reactant and product complexes was mapped with ten replicas using the NEB method for the system in water. The geometry on the top of the NEB reaction pathway was isolated and used for the saddle point search, then a numerical frequency calculation was performed on it to confirm that the transition state has one imaginary frequency.

By optimizing the corresponding displacements of the transition state along the negative frequency mode, the final reactant and product states were determined. Based on the newly found reactant and product, the final NEB reaction pathway with 10 beads along the reaction profile was constructed; after each bead on NEB pathway was optimized in solution, molecular dynamics simulation was performed on each bead to equilibrate the solvent for 40 picoseconds. This procedure was repeated until the final NEB reaction pathway was converged. Then we calculated the PMFs under DFT/MM and CCSD(T)/MM representations in water solution according to Equation (3). The corresponding free energy difference in Equation (3) was calculated using the free energy perturbation theory[38,39]. The free energy difference was first computed in the relatively inexpensive DFT/MM level of theory, then was shifted to the CCSD(T)/MM level of theory to achieve the highly accurate PMF. Before shifting to the CC representation, we calculated the DFT energy using the Hartree–Fock exact exchange functional; then based on the above DFT reference orbitals, we computed the CCSD(T) correlation energy under the CC representation; finally, the total CCSD(T) energy was obtained by adding the two parts' energy together

III. RESULTS AND DISCUSSIONS

Reactant State: The reactants for the $CH_3Br + CN^-$ reaction in the solution phase and in gas phase are both shown in Figure 1. Unlike the reactant complex in gas phase, in which the nucleophile CN^-

forms a straight line with center C atom in the substrate; in solution phase, the nucleophile tilts up to form an angle with the center C atom, ∠CCN = 107.9º. This is understandable as the nucleophile CN^- attracts seven water molecules unevenly distributed around it with an average hydrogen bond distance around 3.00 Å. Note the C-C bond length is 2.98 Å in gas phase, while it is prolonged to 3.25 Å in solution phase due to the charge screening on CN^- by the surrounding waters; in other words, the presence of the water environment reduces the interaction between substrate and the nucleophile in the reactant state. The C-Br distances are almost the same, 2.03 Å and 1.99 Å, in the gas and solution phases. The solvation pattern we observed here is consistent with previous experimental[47] and theoretical studies[38,48-52].

Transition State: Shown in Figure 2，the transition state in water, $(Br\cdots CH_3\cdots CN)^-$, is the highest point (No. 5 bead) on the NEB reaction pathway. Numerical frequency calculations confirmed the presence of single imaginary frequency of 437.9*i* cm^{-1} for the saddle point. The structure of the transition state is characterized by the formation of a nearly planar CH_3 group. We noticed that, ∠CCN changes to 170.0º in transition state from 107.9º in reactant complex; the C-C distance is decreased from 3.25 Å in reactant to 2.34 Å, and the C-Br distance is elongated from 2.03 Å in reactant to 2.38 Å. So it is in the middle of a concerted process of one bond breaking (C-Br) and one bond forming (C-C). We also found that CN^- accepts six hydrogen bonds at transition state.

Product State: At the product state (shown at the bottom of Figure 2), the leaving group Br^- is now broken away from the center of C atom and the distance between them reaches to 3.33 Å. At the mean time, the attacking CN^- group combines CH_3 with a C-C distance at 1.45 Å to form CH_3CN. Thus the synchronized bond-breaking and bond-forming process was finished. Six water molecules surround the attacking CN^- with average N-O distance of 3.20 Å. Here, the solvent caging effect stabilizes the product complex $Br^-\cdots CH_3CN$, which does not exist in the gas phase.

Geometry Evolution along the NEB Reaction Pathway: In this work, we provide the evolution of the reaction process along the NEB reaction path in Figure 3 to explore the detailed reaction mechanism.

Ten snapshots along the NEB reaction pathway display a S_N2 reaction mechanism in aqueous solution: a concerted bond breaking and forming process with the Walden inversion of the CH_3 group. From the reactant Fig. 3.1 to transition state Fig. 3.5, the C-C length has become shorter from 3.25Å to 2.34 Å; while in the mean time, the distance from C to Br has increased from 1.99 Å to 2.38 Å. From the transition state Fig. 3.5 to the product state Fig. 3.10, the C-C distance further decreases from 2.34 Å to 1.45 Å, and the Br-C length further increases from 2.38 Å to 3.33 Å. The synchronized C-Br bond breaking in the substrate and C-C bond forming with the nucleophile represents a S_N2 reaction mechanism in aqueous solution.

Charge Distributions along the NEB Reaction Pathway: Another character of the S_N2 reaction mechanism is the concerted charge transfer process along the reaction pathway. Figure 4 shows the charge redistribution for this reaction of the 10 beads along the NEB reaction pathway. The beads 1, 5, and 10 are the corresponding reactant, transition state and product complex along the pathway. At the reactant state, bead 1, the substrate CH_3Br is neutral, the whole negative charge of -1.0 is on the cyanide ion. As the reaction proceeds to beads 5, the negative charge initially on the cyanide ion has been delocalized so that the charge of the attacking CN lost **-**0.18 and the leaving group Br got -0.25 while the CH_3 has positive charge at +0.36. At the bead 10, compared to the initial charge distribution, the charges on Br and CN have taken a reverse role. The net negative charge of the leaving group Br^- increases to -1.0 while the charge around CN decreased to -0.22, and the new product CH_3CN is neutral now. This concerted charge transfer process guarantees the whole negative charge has been gradually transferred from the nucleophile to the leaving group.

Molecular Dipole Moment along the NEB Reaction Pathway: The molecular dipole moment along the NEB reaction path is presented in figure 5. Here, the unit of the dipole moment is Debye. Note the larger molecular dipole moments are for the geometries on the product side not the reactant side. The first reason is that CH_3CN with a dipole moment 3.92D on the product side is much polar than CH_3Br with a dipole moment 1.82D[53] on the reactant side. the second reason is that $CH_3CN...Br^-$ is more

sloppy in Figure 3.10-7 than their counter parts in Figure 3.1-3. While smallest dipole moments are for the 5th and 6th beads at 2.7 and 1.8D. This is not surprising since, around the transition state region, the charge is delocalized surrounding the whole molecule while the structures are more compact than the reactant and product complexes.

Potential of Mean Force: Figure 6 compares the PMFs between the DFT/MM and CCSD(T)/MM representations for the $CH_3Br + CN^- \rightarrow CH_3CN + Br^-$ in water along the NEB reaction pathway; the solvent contribution (blue line) to the free energy (last term in Eq.3) is also plotted here against the PMF profiles. In aqueous solution, the PMFs of the reaction path are determined directly based on Equation 3. Here the number 1 bead is used as the reference energy point, so only the relative free energies are calculated along the reaction pathway. The results show that the free energy activation barrier is 19.1 kcal/mol under the CCSD(T)/MM representation, which agrees very well with the experimental[30]value in aqueous solution, 20.7 kcal/mol. But under the DFT/MM representation, the barrier height is at 16.5 kcal/mol, which underestimates the activation barrier height by 4.2 kcal/mol compared to the experimental value. This is expected, because DFT method usually underestimates the reaction barrier height comparing to the CC method[54-56] in gas phase for benchmarked S_N2 reactions. This situation still holds true for the reactions in solution phase as demonstrated from the previous studies of the S_N2 reactions[42-47]. Nonetheless, both values are significantly larger compared to the barrier height at 8.9[27] kcal/mol for gas phase, The presence of solution actually weakens the reactivity of this reaction by raising the barrier height 10.4 kcal/mol under the CCSD(T)/MM representation. This figure also shows that the free reaction energy for this reaction is −40.6 kcal/mol at CCSD(T) level theory. We can see that the solvation energy contributes 2.1 kcal/mol for the product respected to the reactant state.

Next, based on the early published results of the solvation energies of CH_3Br (-2.1 kcal/mol)[57], CH_3CN (-3.9 kcal/mol)[58], CN^-(-72.0 kcal/mol)[58] and Br^- (-68.3 kcal/mol)[58] and the gas phase reaction profile[27,28] (barrier height at 8.9 kcal/mol, reaction energy at -43.0 kcal/mol), we can estimate the potential of mean force in solution phase, then compare with our calculated PMF. The comparison

between our calculated PMF reaction profile and the estimated schematic PMF in aqueous solution is schematically plotted in Figure 7. Note, the barrier height of the estimated PMF is adopted from the experimental results[30]; the free reaction energy, -41.1 kcal/mol, in solution phase is obtained from the combining numbers of the solvation energies of CH_3Br, CH_3CN , CN^- and Br^- in gas phase listed above. This figure shows that the PMF obtained from this work (the black line) under the CCSD(T)/MM representation agrees quite well with the estimated PMF (the red line) in aqueous solution: our calculated reaction free energy, -40.6 kcal/mol, agrees very well with the estimated reaction free energy at -41.1 kcal/mol and our calculated free energy barrier height at 19.1 kcal mol/1 also has a quite good agreement with the experimental value at 20.7 kcal/mol.

Solution Contribution: The contributions of aqueous solution on the reaction energy come from two aspects: the solvation effect and polarization effect. We already know, from Figure 6, the solvation effect (blue line) plays a big role on the PMF by contributing ~10.4 kcal/mol to the transition state barrier height. Next, we examine the polarization effect to see which effect plays a dominant role in shaping the PMF. The polarization effect is the perturbation to the solute electronic structures caused by presence of the water solution. It was obtained by comparing the gas-phase energies along the NEB pathway and the solute internal energies at CCSD(T) level in Figure 8. Here, the gas-phase reaction pathway is calculated using the same 10 structures on the NEB pathway in solution but excluding the interaction between the solute and solvent; the internal energy of the QM/MM system is obtained by excluding the solution contribution. Compared to the gas phase, the polarization of solute caused by the solvent raises the energy by ~3.2 kcal/mol, ~7.3 kcal/mol, ~3.3 kcal/mol for reactant state, transition state and product state at the CCSD(T)/MM level of theory. The net result is about a 4.1 kcal/mol increase on the barrier height. In total, the combination of the solvation effect and the polarization effect adds 14.5 kcal/mol to the reaction barrier height respected to the gas-phase. Therefore, about 30% of the contributions from the aqueous solution to transition state is from the polarization effect, about 70% from the solvation effect. Thus we can conclude that, among the two contributions to the PMF from the

aqueous solution, that the solvation effect has a much bigger impact on the PMF compared to the polarization effect.

Comparison with CH_3Br +OH^- Reaction: Using the same above protocol, we have also investigated a similar reaction, $CH_3Br + OH^-$ in aqueous solution[50]. Therefore, we can compare the reaction properties of these two reactions with the same substrate but different nucleophiles in water solution. According to our results in water, under the CCSD(T)/MM level of theory, the barrier heights for the two reactions are 22.8 kcal/mol for the $CH_3Br + OH^-$ and 19.1 kcal/mol for the $CH_3Br + CN^-$ respectively, which means that CN^- is a better nucleophile than OH^- to repel Br from the substrate. This is verified by empirical measures of nucleophilicity that CN^- has a bigger nucleophilic constant[59] at 6.7 than OH^- at 6.5[60-62].

Our results also show that the presence of the water solution raises the activation barrier height by 16.2 kcal/mol for the $CH_3Br + OH^-$; However, it only raises 14.5 kcal/mol for the $CH_3Br + CN^-$. This is expected since OH^- has a larger hardness parameter at 5.6 than CN^- at 5.3[63]; In other words, OH^- anion has a more localized charge than CN^-; Consequently, OH^- is better solvated than CN^-, thus OH^- lowers more energy of the nucleophile in water relative to the transition state; thereupon, OH^- under the presence of water raises the barrier height more than CN^- does.

Furthermore, both calculations show the activation barrier heights, calculated under the CCSD(T)/MM level theory, agree with experimental values very well. Along with the above comparison, the current multilayered-representation protocol provides a way to not only correctly describe the characters of the S_N2 reaction but also accurately compute the PMF under the CCSD(T) level of theory, as well as to predict the solvent effect contributions to the PMF along the reaction pathway.

IV. CONCLUSION

The $CH_3Br + CN^-$ reaction in aqueous solution was investigated using a multilayered-representation

QM/MM methodology. By employing three different representations, DFT/MM, CCSD(T)/MM and ESP/MM, we shifted the huge computational cost of statistical sampling to the less expensive DFT/MM, and ESP/MM representations, then finally obtained the accurate PMF under the CCSD(T)/MM representation. Reactant complex, transition states, and product complex have been identified and characterized. Due to the solvent screening effect, the interaction between the substrate and the nucleophile is decreased comparing to gas phase. The detailed plot of the configuration evolution along the reaction pathway reveals a synchronized C-Br bond breaking and C-CN bond forming process, as well as a CH_3 Walder inversion process. Thus this reaction in solution phase presents a standard S_N2 reaction mechanism. Not only the bond breaking and forming is synchronized but also the charge transfer process is synchronized along the neb reaction pathway: the net negative charge of the leaving group Br^- increases to -1.0 while the charge around CN decreased to -0.22 concertedly. The molecular dipole moments on the product sides are bigger than those on the reactants since the molecules on the product side are more sloppy than on the reactant side and the substrates on the product side have bigger dipole moments than those on the reactant sides.

The PMF shows an activation barrier height, at the accurate CCSD(T)/MM theory, is 19.1 kcal/mol, which agrees very well with the experimental measure value of 20.7 kcal/mol. But the DFT/MM representation underestimates the reaction barrier height, which gives a reaction barrier height of 16.5 kcal/mol. The computation tells us that the aqueous environment contribute greatly to the PMF: the solvation effect and polarization effect combined contribute about 14.5 kcal/mol to the activation barrier respect to that in gas phase. Among the two solvent contributions, the solvation effect plays the major role by dominating 70% of the contribution, while the polarization effect contributes the rest. The increase of the activation barrier height in the aqueous solution respect to gas phase indicates that the reactivity is greatly affected by the aqueous environment for this reaction.

ACKNOWLEDGMENTS

D. Y. Wang thanks the National Natural Science Foundation of China (Grant #: 11374194) and Taishan Scholarship fund for supporting this work. The computation work was carried out at the National Supercomputing Center in Shenzhen.

References

(1) D. C. Clary, J. Palma, *J. Chem. Phys*, 1997, **106**(2), 575.

(2) J. Kenyon, H. Phillips, *Trans. Faraday Soc*, 1930, **26**, 451.

(3) T. V. Venkitachalam, P. Das, R. Bersohn, *J. Am. Chem. Soc*, 1983, **105**(25), 7452.

(4) E. D. Hughes, *Trans. Faraday Soc*, 1938, **34**, 202.

(5) A. P. Wolf, P. Schueler, R. P. Pettijohn, et al, *J. Phys. Chem*, 1979, **83**(10), 1237.

(6) A. P. Bento, F. M. Bickelhaupt, *J. Org.Chem*, 2007, **72**(6), 2201.

(7) L. Sun, W. L. Hase, K. Song, *J. Am. Chem. Soc*, 2001, **123**(24), 5753.

(8) C. H. DePuy, S. Gronert, A. Mullin, V. M. Bierbaum, *J. Am. Chem. Soc*, 1990, **112**(24),8650.

(9) J. Chandrasekhar, W. L. Jorgensen, *J. Am. Chem. Soc*, 1985, **107**(10), 2974.

(10) R. C. Dougherty, *Org Mass Spectrometry*, 1974, **8**(1), 85.

(11) G. Caldwell, T. F. Magnera, P. Kebarle, *J. Am. Chem. Soc*, 1984, **106**(4), 959.

(12) T. F. Magnera, G. Caldwell, J. Sunner, S. Ikuta, P. Kebarle, *J. Am. Chem. Soc*, 1984, **106**(21), 6140.

(13) K. Ando, J. T. Hynes, *J. Phys. Chem. B*, 1997**, 101**(49)*,* 10464.

(14) W. J. Albery, M. M. Kreevoy, *Adv. Phys. Org. Chem*, 1978, **16**, 85.

(15) S. Kato, G. E. Davico, H. S. Lee, C. H. DePuy, V. M. Bierbaum, *Int.J. Mass Spectrom*, 2001, **210**, 223.

(16) A. Dedieu, A. Veillard, *J. Am. Chem. Soc*,1972, **94**, 6730.

(17) A. A. Viggiano, J. S. Paschkewitz, R. A Morris, J. F. Paulson, A. Gonzalez-Lafont, D. G. Truhlar, *J. Am. Chem. Soc*, 1991, **113**, 9404.

(18) S. Shaik, A. Ioffe,A. C. Reddy, A. Pross, *J. Am. Chem. Soc*. 1994, **116**, 262.

(19) S. S. Shaik, P. C. Hiberty, *Adv. Quantum Chem.* 1995, ***26***, 99.

(20) p. Manikandan, J. X. Zhang, W. L.Hase, *J. Phys. Chem. A*, 2012, **116**, 3061

(21) J. Mikosch, S. Trippel, C. Eichhorn, R. Otto, U. Lourderaj, J. X. Zhang, W. L. Hase, M. Weidemuller, R. Wester, *Science*, 2008, **319**, 183

(22) J. X. Zhang, J.Mikosch, *S.* Trippel, R. Otto*,* M. Weidemuller, R. Wester, W. L. Hase , *J. Phys. Chem. Lett*, 2010, **1**, 2747

(23) J. Mikosch, J. X. Zhang, *S.* Trippel, C. Eichhorn, R. Otto, R. Sun, W. A. de Jong, M. Weidemuller, W. L. Hase, R. Wester *, J. Am. Chem. Soc*, 2013, **135**, 4250.

(24) J. X. Zhang, U. Lourderaj*,* R. Sun, J. Mikosch, R. Wester. W. L. Hase, *J. Chem. Phys*., 2013, **138**, 114309 .

(25) J. Xie, R. Sun, M. R. Siebert, R. Otto, R. Wester, W. L. Hase, *J. Phys. Chem. A*, 2012, **117**, 7162.

(26) D. K.Bohme, G. I. Mackay, *J. Am. Chem. Soc*, 1981, **103**(4), 978.

(27) S. S. Shaik, H. B. Schlegel, S. Wolfe, *Theoretical Aspects of Physical Organic Chemistry: The S_N2 Mechanism*, Wiley, New York, 1992.

(28) K.Tanaka, G. I.Mackay, J. D.Payzant, D. K.Bohme, *Can. J. Chem,* 1976, **54**, 1643.

(29) B. Safi, K. Choho, and P. Geerlings, *J. Phys. Chem. A*, 2001**, 105***,* 591.

(30) B. W. Marshall, E. A. Moelwyn-Hughes, *J. Chem. Soc (Resumed)*, 1965, 7119.

(31) J. L Gao, D. G. Truhlar*, Annu. Rev. Phys. Chem.*, 2002, **53**, 467.

(32) A. Warshel, *Annu. Rev. Biophys. Biomol. Struct*, 2003, **32**, 425.

(33) A. Warshel, M. J. Levitt, *Mol. Biol*. 1976, **103(2)**, 227.

(34) P. Hohenberg, and W. Kohn, *Phys. Rev*, 1964,**136**, B864.

(35) R. J. Bartlett, J. F. Stanton, *Rev. Comput. Chem*, 1993, **5**, 65.

(36) R. J. Bartlett, and M. Musial, Rev. *Mod. Phys*. 2007, **79**, 271.

(37) M. Valiev, B. C. Garrett, M. K. Tsai, K. Kowalski, S. M. Kathmann, G. K. Schenter, and M. Dupuis, *J. Chem. Phys*, 2007, **127**, 051102.

(38) D.Y. Wang, M. Valiev, and B. C. Garrett, *J.Phys.Chem. A*. 2011,**115**, 1380.

(39) M. Valiev, E. J. Bylaska, N. Govind, K. Kowalski, T.P. Straatsma, H. J.J. van Dam, D. Wang, J. Nieplocha., E. Apra, T.L. Windus, and W.A. de Jong, *Comput. Phys. Commun*, 2010, **181**,1477.

(40) Y. K. Zhang, H. Y. Liu, and W. T. Yang, *J. Chem. Phys*, 2000, **112**, 3483.

(41) H. J. C Berendsen, J. R. Grigera, T. P. Straatsma, *J. Phys. Chem*. 1987, **91**, 6269.

(42) C. Lee, W. Yang, and R. G. Parr, *Phys. Rev. B*. 1988, **37**, 785.

(43) A. D. Becke, *J. Chem. Phys.* 1993, **98**, 5648.

(44) T. Fox, and P. A. Kollman, *J. Phys. Chem. B*. 1998, **102**, 8070.

(45) G. Henkelman, B. P. Uberuaga, H. A. Jónsson, *J. Chem. Phys*, 2000, **113**, 9901.

(46) D. Sheppard, R. Rerrell, G. Henkelman, *J. Chem. Phys, 2008*, **128**, 134106.

(47) A. Botti, F. Brunti, S. Imberti, M. A. Ricci, and A. K. Soper, *J. Mol. Liq*, 2005, **117**, 81.

(48) H.Y. Yin, D. Y. Wang, and M. Valiev, *J. Phys. Chem. A*. 2011, **115**, 12047.

(49) T. T. Wang, H.Y. Yin, D. Y. Wang, and M. Valiev, *J. Phys. Chem. A*, 2012,**116**, 2371.

(50) Y.L. Xu, T.T. Wang, D. Y. Wang, *J. Chem. Phys*. 2012, **137**, 184501 .

(51) J. Chen, Y. Xu, D. Wang, *J. Comput. Chem*, 2014, **35**(6),445.

(52) J. Zhang, Y. Xu, J. Chen, D. Wang, *Phys. Chem. Chem. Phys*, 2014, **16,** 7611**.**

(53) Jr. R. D. Nelson, Jr. D. R. Lide, A. A. Maryott. Selected values of electric dipole moments for molecules in the gas phase[R], NATIONAL STANDARD REFERENCE DATA SYSTEM, 1967.

(54) J. M. Gonzales, C. Pak, R. S. Cox, W. D. Allen, H. F. Schaefer, A. G.Csaszar, G. Tarczay, *Chem. Eur. J*, 2003, **9**, 2173.

(55) J. M. Gonzales, R. S. Cox, S. T. Brown, W. D. Allen, H. F. Schaefer, *J. Phys. Chem. A*, 2001, **105**, 11327.

(56)Y. Zhao, N. Gonzalez-Garcia, D. G. Truhlar, *J. Phys. Chem. A* 2005, **109**,2012.

(57) S. S. Shaik, W. Wu, K. Dong, et al, *J. Phys. Chem. A*, 2001, **105**(35), 8226.

(58) Jr. J. R. Pliego, J. M. Riveros , *Chem. Phys. Lett*, 2000, **332**(5), 597.

(59) C. G. Swain and C. B. Scott, *J. Am. Chem. Soc*, 1953, **75**, 141.

(60) R. G. Pearson and J. Songstad, *J. Am. Chem. Soc,* 1967, **89**, 1827.;

(61) R. G. Pearson, H. Sobel, and J. Songstad, *J. Am. Chem. Soc,* 1968, **90**, 319.

(62) P. L. Bock and G. M Whitesides, *J. Am. Chem. Soc,* 1974, **96**, 2826.

(63) R. G. Parr and R. G. Pearson, *J. Am. Chem. Soc,* 1983, **105**, 7512.

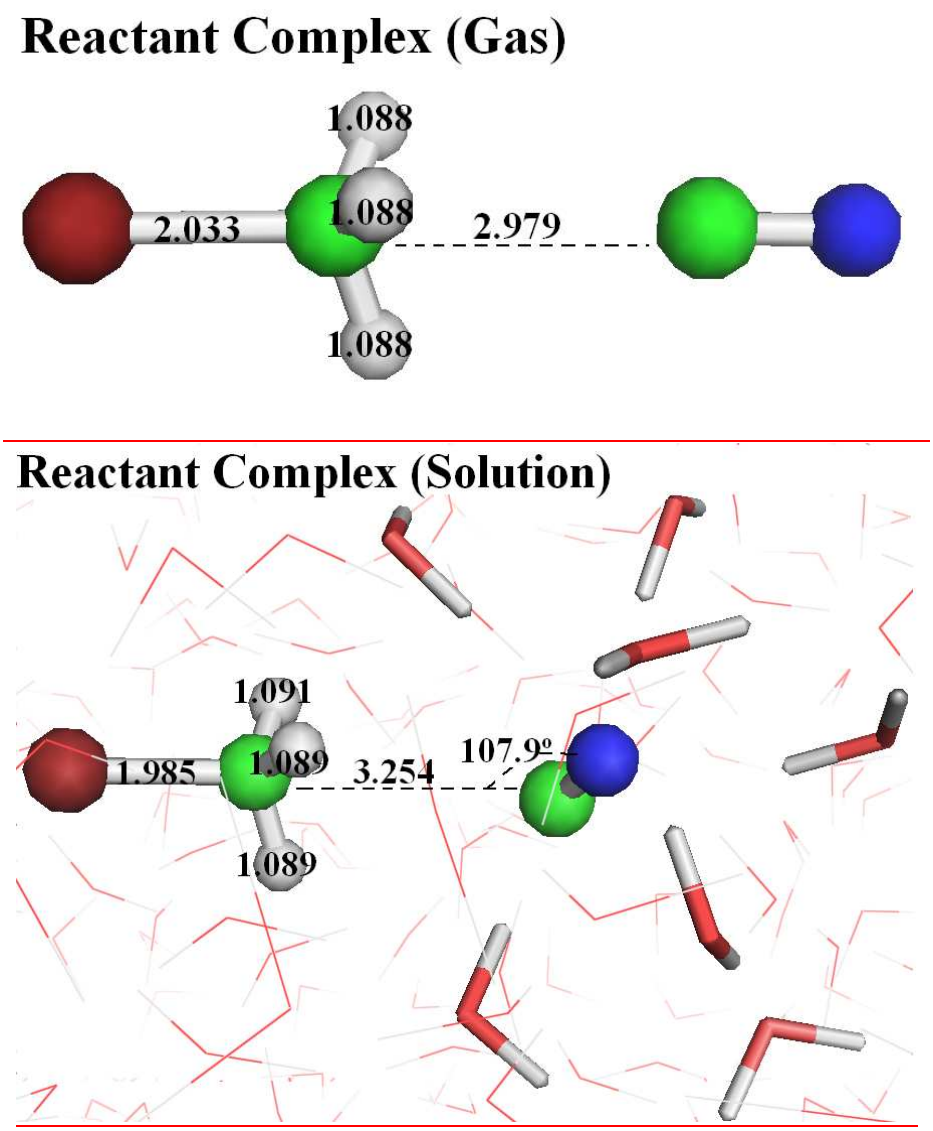

Figure 1. Structures of the reactant complex for the reaction $CH_3Br + CN^- \rightarrow CH_3CN + Br^-$ in gas phase and in aqueous solution. The indicated distances are in Angstroms.

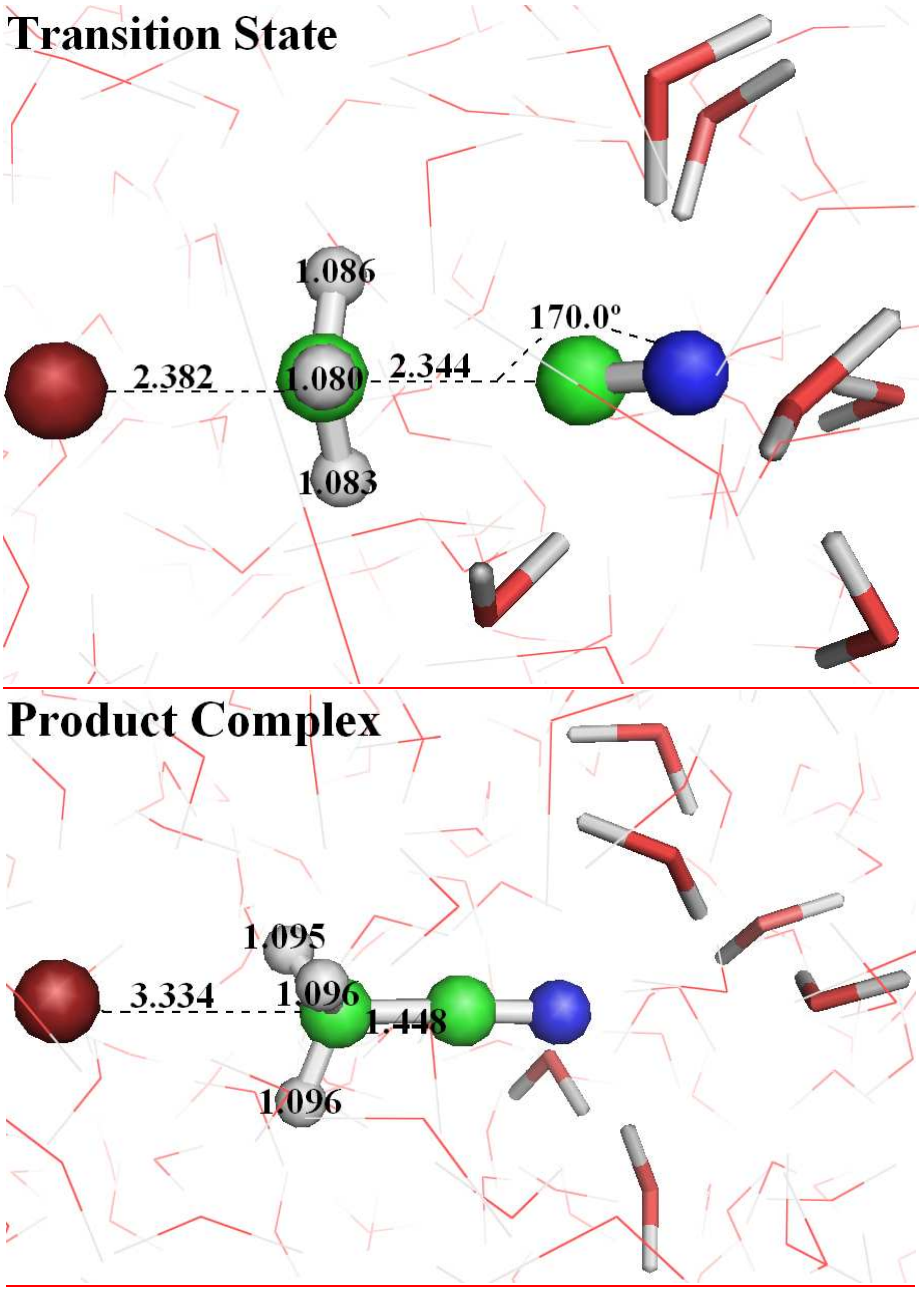

Figure 2. Structures of the transition state, and product complex for the reaction $CH_3Br + CN^- \rightarrow CH_3CN + Br^-$ in aqueous phase. The indicated distances are in Angstroms.

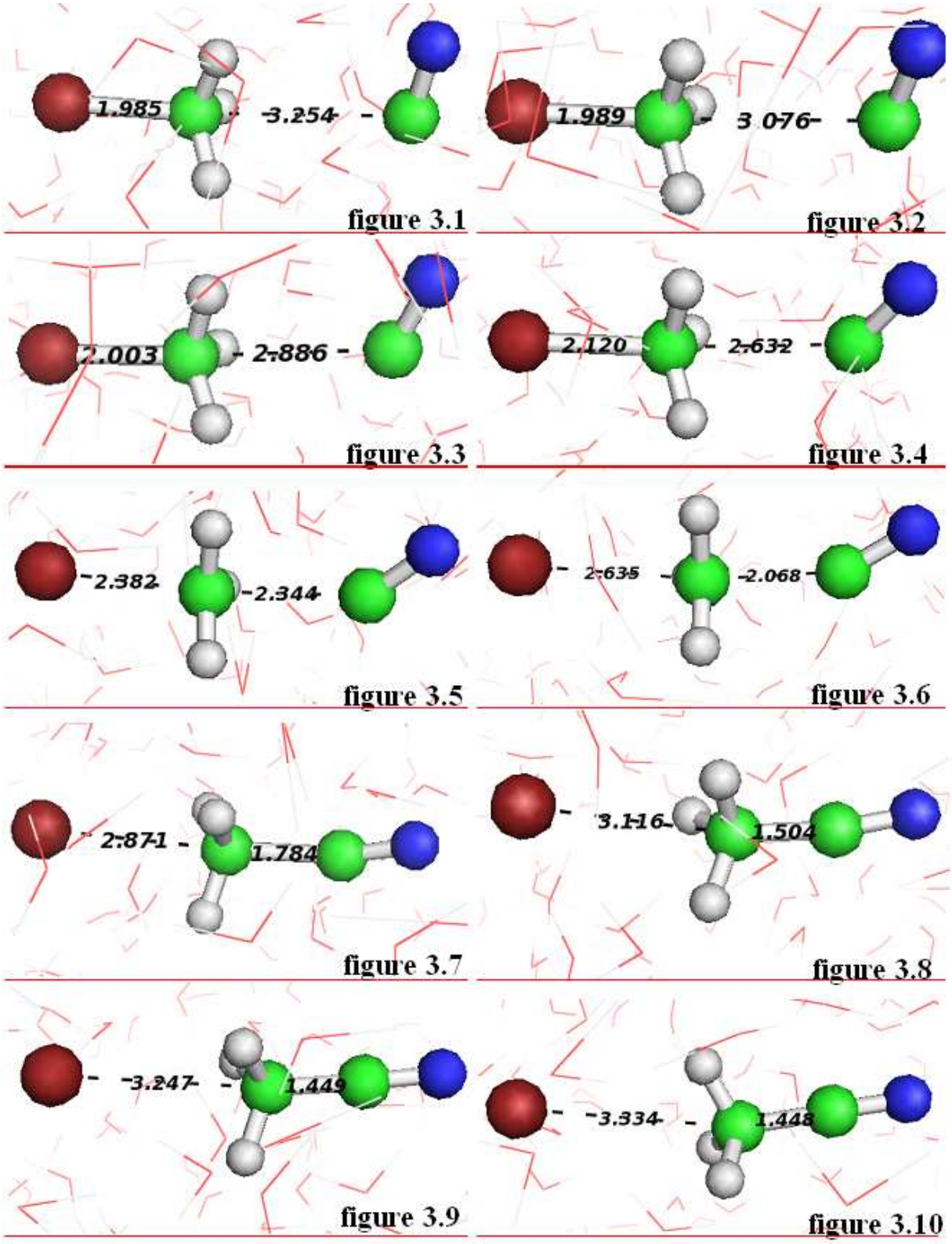

Figure 3. Structures of the ten beads along the NEB reaction pathway for $CH_3Br + CN^- \rightarrow CH_3CN + Br^-$ in aqueous solution. No. 1 is the structure of the reactant state, No. 5 is the transition state, and No.10 is the product state for the reaction. The indicated distances are in Angstroms.

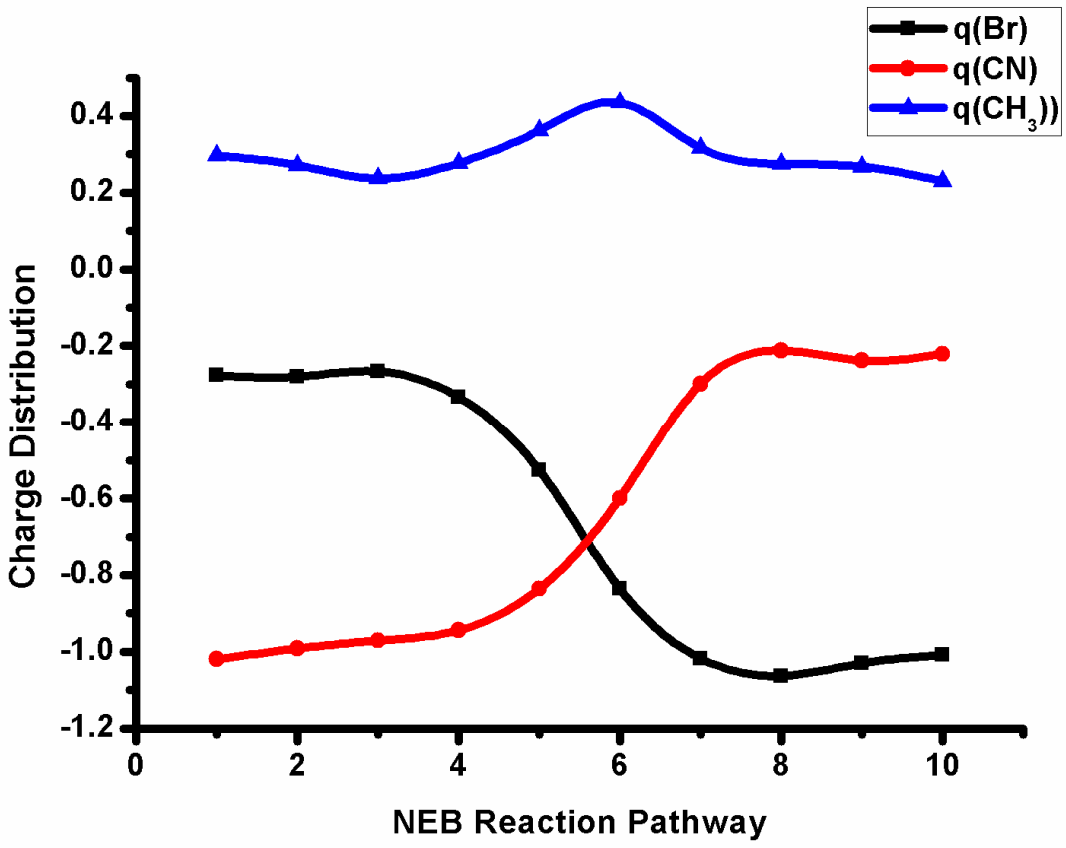

Figure 4. Charge distributions of the CH_3, CN and Br along the NEB reaction pathway for the reaction $CH_3Br + CN^- \rightarrow CH_3CN + Br^-$.

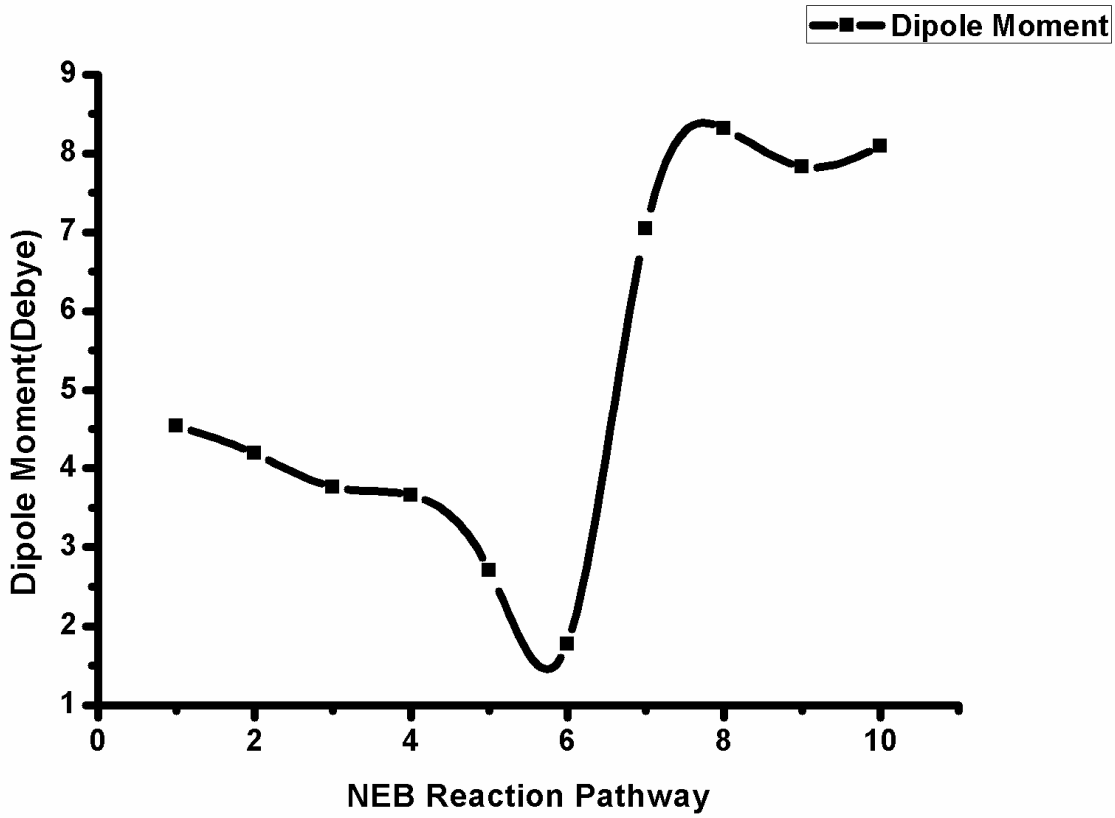

Figure 5. Dipole moment of the CH_3, CN and Br along the NEB reaction pathway for the reaction $CH_3Br + CN^- \rightarrow CH_3CN + Br^-$.

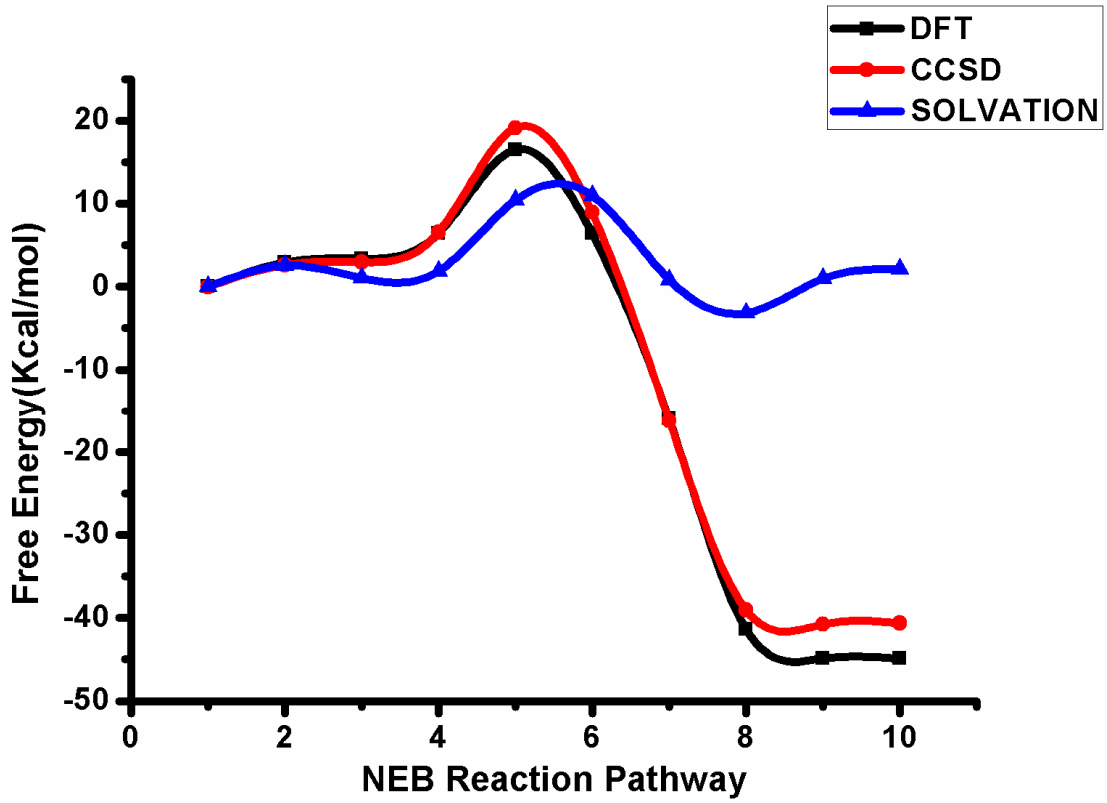

Figure 6. Comparison of the potential of mean force calculated at DFT/MM and CCSD(T)/MM levels of theory and solvation contribution using the reactant state (bead 1) as a reference point.

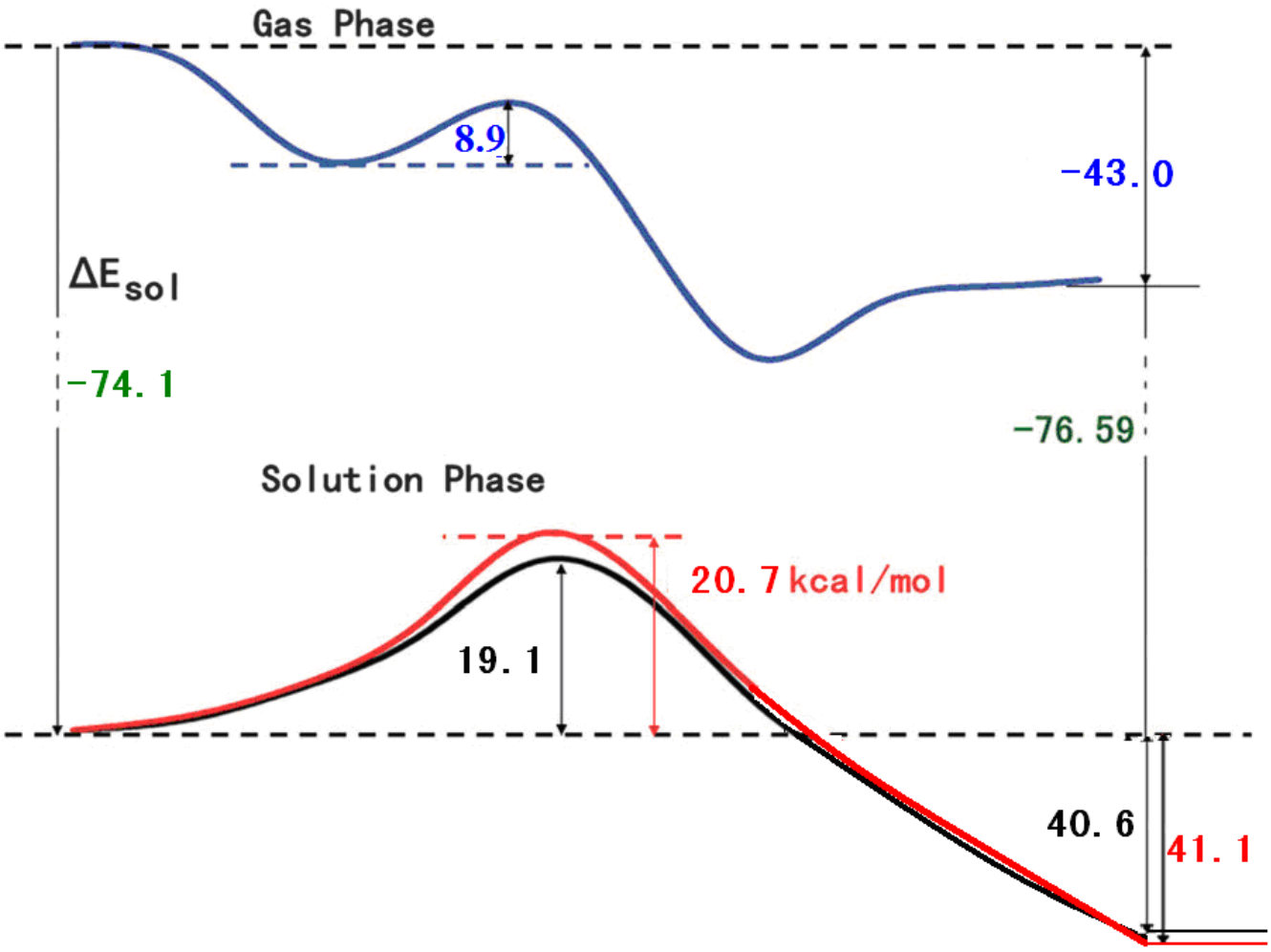

Figure 7. Comparison of schematic free energy profiles in the gas phase (blue curve) and in aqueous solution (The black curve is the PMF calculated at the CCSD(T)/MM level of theory; red is the estimated one using the gas-phase reaction energy[27] and solvation energies of the reactant and the product[57,58], the experimental activation barrier height, 20.7 kcal/mol, is taken from ref[30].).

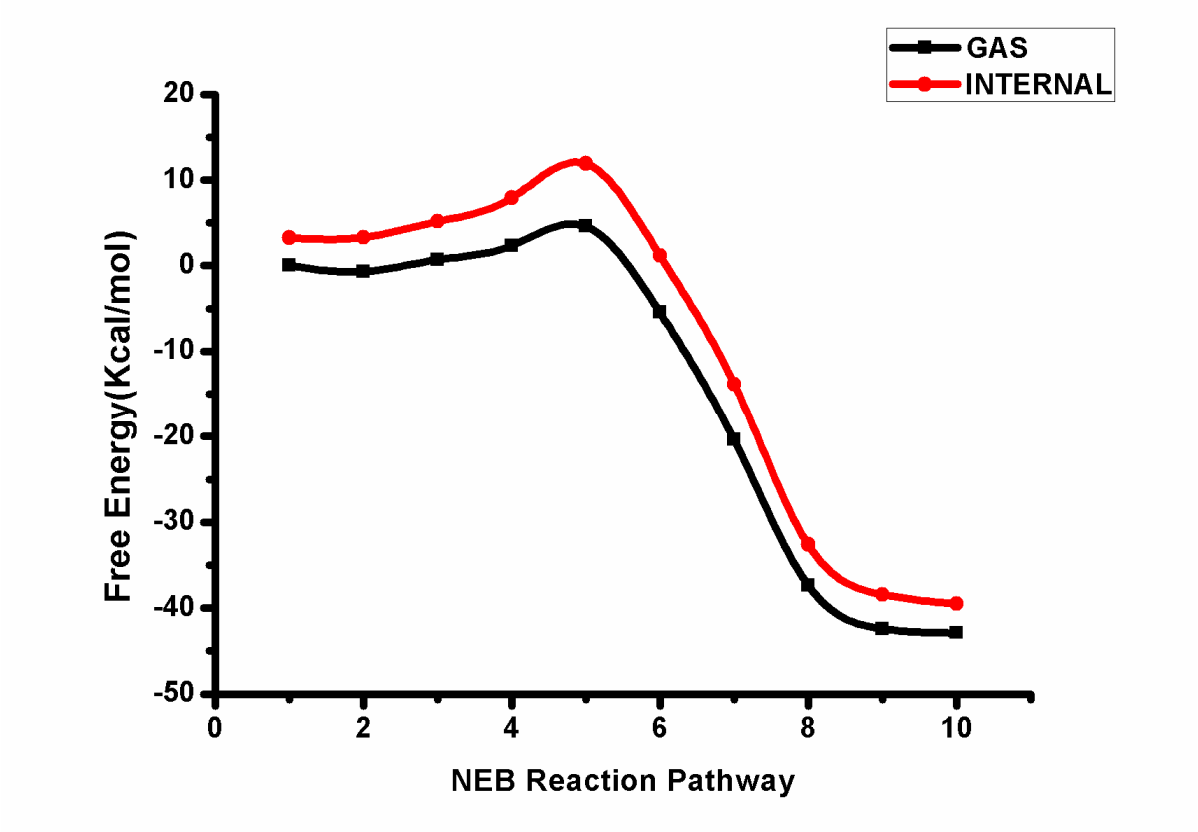

Figure 8. Comparison between gas-phase and solute internal energies along the NEB reaction pathway under the CCSD(T)/MM representation using the gas-phase energy of the reactant state as a reference point

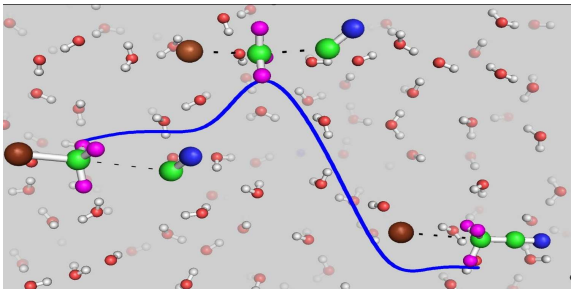

The potential of mean force for the $CH_3Br + CN^-$ reaction was obtained under the CCSD(T)/MM level of theory using a multilayered-representation quantum mechanical/molecular mechanics approach, as well as the reactant, transition state and product complexes along the reaction pathway in aqueous solution.